Coupling lattice Boltzmann and molecular dynamics models for dense fluids

A. Dupuis, E. M. Kotsalis, and P. Koumoutsakos
Computational Laboratory, ETH, Zurich CH-8092, Switzerland
(Received 27 October 2006; revised manuscript received 12 February 2007; published 11 April 2007)

We propose a hybrid model, coupling lattice Boltzmann (LB) and molecular dynamics (MD) models, for the simulation of dense fluids. Time and length scales are decoupled by using an iterative Schwarz domain decomposition algorithm. The MD and LB formulations communicate via the exchange of velocities and velocity gradients at the interface. We validate the present LB-MD model in simulations of two- and three-dimensional flows of liquid argon past and through a carbon nanotube. Comparisons with existing hybrid algorithms and with reference MD solutions demonstrate the validity of the present approach.

DOI: 10.1103/PhysRevE.75.046704 PACS number(s): 47.11.−j, 82.20.Wt, 83.50.Lh, 83.10.Mj

I. INTRODUCTION

The advent of nanotechnology provides us today with nanoscale devices that can affect flow phenomena that are important for several technological applications. Examples include microfluidic channels with nanopatterned walls, biosensors embedded in aqueous environments [1–4], or bluff bodies with superhydrophobic surfaces [5].

The detailed investigation of flow physics at the nanoscale has been pioneered by Koplik [6] using molecular dynamics (MD) models. When nanoscale devices are active parts of microscale and macroscale systems, a multiscale approach is required to integrate atomistic simulations with computational methods suitable for modeling of flow phenomena at larger scales. A number of hybrid models coupling atomistic to continuum descriptions of dense fluids have been proposed [7–12].

O'Connell and Thompson [7] coupled an atomistic with a continuum system where the average momentum of the overlap particles is adjusted through a boundary force. Flekkøy *et al.* [9] presented a model based on direct flux exchange between atomistic and continuum regions. Hadjiconstantinou and Patera [8] proposed to decouple time scales by using the Schwarz domain decomposition method coupling an atomistic to a continuum description of a fluid. Convergence to a steady state solution is achieved through alternating iterations between steady state solutions within the atomistic and continuum subdomains. Nie *et al.* [10,13] employed a domain decomposition algorithm to simulate Couette flow over a nanopatterned surface, as well as a cavity flow where the domain at the corner of the static and the moving walls was described atomistically. The use of atomistic descriptions offers a natural way to overcome singularities (such as the description of the velocity field at the corners of the cavity problem) associated with continuum descriptions. At the same time new challenges emerge as, for example, the absence of periodicity in MD simulations. The absence of periodicity is often associated with disturbances in the homogeneity of the atomistic region. Nie *et al.* [10,13], following the work of O'Connell and Thompson [7] proposed the use of a singular boundary force in order to compensate for the elimination of periodicity in the MD system. Werder *et al.* [11] proposed an algorithm using the alternating Schwarz method to couple an MD model for liquid argon to an incompressible Navier-Stokes (NS) finite volume solver. A boundary force was developed that takes into account the physical properties of the fluid that is being simulated. They reported on simulations of flows past a carbon nanotube (CNT) and noticed average departures from reference MD simulations of the order of 4%.

Here we extend the model proposed in [11] by coupling the MD simulations with a lattice Boltzmann (LB) method [14] of the incompressible NS equations. The proposed extension aims to take advantage of the mesoscopic modeling inherent in LB simulations and to allow for a broader geometric flexibility than the one allowed by the finite volume solver. In addition, in the present work we enhance the exchange between atomistic and continuum domains by communicating, in addition to velocities, velocity gradients.

The paper is organized as follows. In Sec. II, we describe the hybrid model by outlining the MD and LB methods and describe their coupling. Results of liquid argon flows past and through a CNT are presented in Sec. III. We compare the results of the hybrid simulations to the reference MD solutions, we discuss the computational efficiency of the hybrid model and conclude in Sec. IV.

II. LB-MD MODEL

In the present hybrid method an MD model describes the flow of liquid argon in the vicinity of a carbon nanotube while a LB approach is used to simulate the behavior of the continuum system away from the CNT.

A. Molecular dynamics

The atomistic region is described by MD simulations where the positions $\mathbf{r}_i=(x_i,y_i,z_i)$ and velocities $\mathbf{u}_i=(u_{x,i},u_{y,i},u_{z,i})$ of the particles evolve according to Newton's equations of motion

$$\frac{d}{dt}\mathbf{r}_i=\mathbf{u}_i \quad \text{and} \quad m_i\frac{d}{dt}\mathbf{u}_i=\mathbf{F}_i=-\sum_{j\neq i}\nabla U(r_{ij}), \qquad (1)$$

where $\mathbf{F}_i$ and m_i are the force and mass of particle i, and r_{ij} is the distance between the particle $\mathbf{r}_i$ and $\mathbf{r}_j$. Here we consider Lennard-Jones (LJ) model of argon interacting with CNTs. The potential $U(r_{ij})$ is defined as

$$U(r_{ij}) = 4\epsilon_{AB}\left[\left(\frac{\sigma_{AB}}{r_{ij}}\right)^{12} - \left(\frac{\sigma_{AB}}{r_{ij}}\right)^{6}\right] + U_b(r_w,\rho,T), \quad (2)$$

where ϵ_{AB} and σ_{AB} are energy and length parameters, A and B denote species. The LJ interaction parameters for argon-argon and argon-carbon interactions are, respectively, $\epsilon_{\mathrm{ArAr}}=0.996$ kJ mol^{-1}, $\sigma_{\mathrm{ArAr}}=0.340$ nm, $\epsilon_{\mathrm{ArC}}=0.570$ kJ mol^{-1}, $\sigma_{\mathrm{ArC}}=0.339$ nm. The coefficients of the Ar-C interactions are derived from second-order Møler-Plesset (MP2) calculations in order to match the binding energy of argon to a benzene ring as a function of the distance. The term U_b is the boundary potential and accounts for the interaction of the boundary region with the surrounding medium. It is further described in Sec. II C. The CNT is modeled as a rigid structure to facilitate the investigation of the flow of argon. All interaction potentials are truncated for distances beyond a cutoff radius $r_c=1.0$ nm. The equations of motion (2) are integrated using a leap-frog scheme with a time step $\delta t=10$ fs.

A desired velocity $\mathbf{u}_d$ is imposed by relaxing the center-of-mass velocity $\bar{\mathbf{u}}_k=1/N_k\Sigma_{i\in k}\mathbf{u}_i$ of the N_k particles within a cell k towards $\mathbf{u}_d$ according to a parameter λ. The velocities $\mathbf{u}_i$ of the particles in the cell k are updated as

$$\mathbf{u}_i = \mathbf{u}_i + \lambda(\mathbf{u}_d - \bar{\mathbf{u}}_k). \quad (3)$$

The slower the velocity relaxes towards its desired value the smaller the amount of perturbations introduced in the system. On the other hand, choosing a small value of λ increases the number of iterations to reach equilibrium and thus decreases the computational efficiency. Here we choose as a relaxation parameter $\lambda=0.1$.

B. Lattice Boltzmann model for the Navier-Stokes equations

The continuum hydrodynamics are described by the incompressible Navier-Stokes equations

$$\frac{\partial \mathbf{u}}{\partial t} + (\mathbf{u}\cdot\nabla)\mathbf{u} = -\nabla p/\rho + \nu\nabla^2\mathbf{u} + \mathbf{g}, \quad (4)$$

$$\nabla\cdot\mathbf{u} = 0, \quad (5)$$

where $\mathbf{u}$ is the fluid velocity, p the pressure, ρ the density, and $\mathbf{g}$ a body force. We use $\mathbf{g}$ to enforce Dirichlet boundary conditions, see discussion below.

The Navier-Stokes equations (4) and (5) are solved using a lattice Boltzmann algorithm [14]. This approach follows the evolution of particle distribution functions f_i on a d-dimensional regular lattice with z links at each lattice point $\mathbf{r}$. The label i denotes velocity directions and runs between 0 and z. $DdQz+1$ is a standard lattice topology classification. The $D3Q15$ lattice we use here has the following velocity vectors $\mathbf{v}_i$: $(0,0,0)$, $(\pm1,\pm1,\pm1)$, $(\pm1,0,0)$, $(0,\pm1,0)$, $(0,0,\pm1)$ in lattice units.

The lattice Boltzmann dynamics are given by

$$f_i(\mathbf{r}+\Delta t\mathbf{v}_i, t+\Delta t) = f_i(\mathbf{r},t) + \frac{1}{\tau}(f_i^{\mathrm{eq}}(\mathbf{r},t) - f_i(\mathbf{r},t)) + \Delta t g i, \quad (6)$$

where Δt is the time step of the simulation, τ is the relaxation time. The equilibrium distribution function f_i^{eq} is a function of the density ρ and the fluid velocity $\mathbf{u}$ defined as

$$\rho = \sum_{i=0}^{z} f_i, \quad \rho\mathbf{u} = \sum_{i=0}^{z} f_i\mathbf{v}_i + \frac{\Delta t}{2}\mathbf{g}. \quad (7)$$

The equilibrium distribution function is chosen as

$$f_i^{\mathrm{eq}}(\mathbf{r},t) = w_i\rho\left(1 + \frac{\mathbf{v}_i\cdot\mathbf{u}}{c_s^2} + \frac{(\mathbf{v}_i\cdot\mathbf{u})^2}{2c_s^4} - \frac{\mathbf{u}^2}{2c_s^2}\right), \quad (8)$$

where $c_s=1/\sqrt{3}$ is the speed of sound and w_i are weights chosen as $w_0=4/9$, $w_i=1/9$ for $i=1-6$ and $w_i=1/72$ for $i=7-14$. The forcing term is defined as [15]

$$g_i = \left(1 - \frac{1}{2\tau}\right)w_i\rho\left(\frac{\mathbf{v}_i-\mathbf{u}}{c_s^2} + \frac{(\mathbf{v}_i\cdot\mathbf{u})}{c_s^4}\mathbf{v}_i\right)\cdot\mathbf{g}. \quad (9)$$

Performing a Chapman-Enskog expansion on the LB dynamics [16] shows that Eqs. (4) and (5) are recovered with a kinematic viscosity expressed as

$$\nu = \frac{(\Delta\mathbf{r})^2}{\Delta t}\frac{1}{3}\left(\tau - \frac{1}{2}\right), \quad (10)$$

where $\Delta\mathbf{r}$ is the lattice spacing.

We enforce Dirichlet boundary conditions using a local forcing term $\mathbf{g}$. The governing equation (4) is rewritten as

$$\frac{\partial\mathbf{u}}{\partial t} = \frac{\mathbf{u}^*(\mathbf{r},t+\Delta t) - \mathbf{u}(\mathbf{r},t)}{\Delta t} = -(\mathbf{u}\cdot\nabla)\mathbf{u} - \nabla p + \nu\nabla^2\mathbf{u} = \mathcal{R} \quad (11)$$

where $\mathbf{u}^*$ is the velocity at time $t+\Delta t$ with no forcing term considered. Including a forcing term leads to

$$\frac{\mathbf{u}^d(\mathbf{r},t+\Delta t) - \mathbf{u}(\mathbf{r},t)}{\Delta t} = \mathcal{R} + \mathbf{g}(\mathbf{r},t), \quad (12)$$

where $\mathbf{u}^d$ is the desired velocity. Subtracting Eqs. (11) from (12) leads to an expression for the forcing term

$$\mathbf{g}(\mathbf{r},t) = \frac{\mathbf{u}^d(\mathbf{r},t+\Delta t) - \mathbf{u}^*(\mathbf{r},t+\Delta t)}{\Delta t}. \quad (13)$$

We note that evaluating $\mathbf{u}^*$ within an LB method consists only of performing a streaming step. Indeed by construction of the equilibrium distribution function ($\rho\mathbf{u}=\Sigma f_i^{\mathrm{eq}}\mathbf{v}_i$, see [16] for details), the second term of the right-hand side of Eq. (6) does not change the velocity $\mathbf{u}$.

C. Hybrid model

We implement a domain decomposition algorithm, based on the Schwarz alternating method [17], to couple the MD description of a dense fluid with an LB model solving the incompressible NS equations. The computational domain is

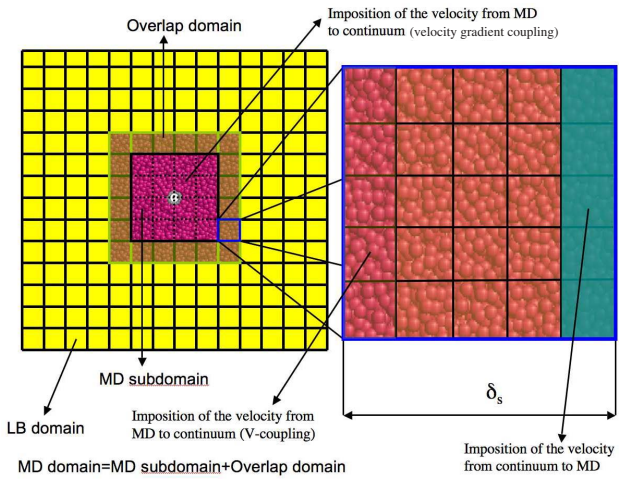

FIG. 1. (Color online) Domain decomposition. The converged solution is obtained by alternating iterations in the LB and MD domains. We consider two ways for imposing the velocity boundary condition from the MD to the continuum. In the case of velocity coupling, we pass the velocities within a one-cell wide strip located at distance δ_s from the end of the MD domain. In the case of the VG coupling we impose MD velocities on every common cell except within a strip of width δ_s close to the boundary.

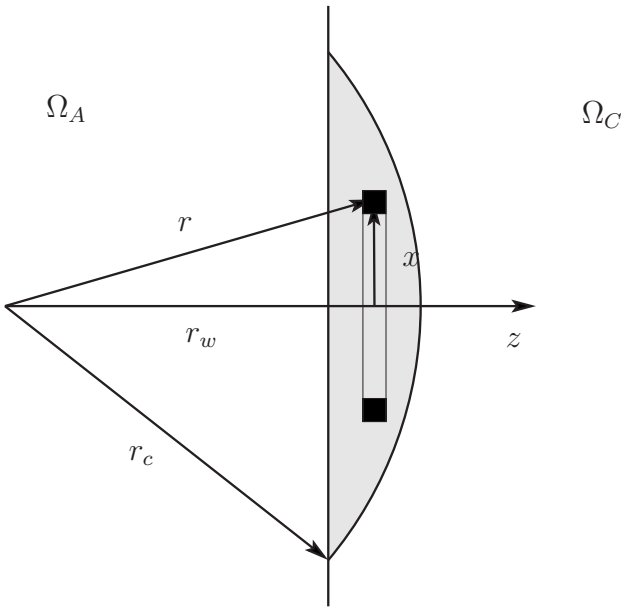

FIG. 2. Integration domains for the effective boundary force [Eq. (14)]. The force contributions along z are integrated over the shaded area. The number of atoms in the infinitesimal ring element is $2\pi\rho_n g(r)xdxdz$, where ρ_n is the average number density and $g(r)$ is the radial distribution function. Ω_A and Ω_C denote the atomistic and the continuum domains, respectively.

decomposed into two overlapping regions: an atomistic region described by molecular dynamics and a continuum region described by the LB model of the incompressible Navier-Stokes equations. The key assumption of our approach is that this decomposition of the system is valid and that the two descriptions match in the overlap domain (see Fig. 1). A Schwarz iteration t_c consists of computing the continuum velocity field $\mathbf{u}_c(t_c)$ with boundary conditions set by the previous atomistic cycle $\mathbf{u}_a(t_c-1)$ and an external boundary condition that depends on the system considered. Then, $\mathbf{u}_c(t_c)$ is used to set the boundary condition for computing $\mathbf{u}_a(t_c)$.

The coupling of the atomistic and the LB domain introduces several challenges that need to be addressed, namely: the absence of periodic boundary conditions in the MD simulations, the sampling of the MD solution over small regions in order to serve as a boundary condition for the continuum and in turn the imposition of the continuum boundary conditions onto each cell of the atomistic domain.

The absence of periodicity in MD simulations of dense fluids requires a mechanism to compensate for particles that exit the boundary. Simplified models such as elastic boundaries and/or particle reinsertion often result in strong density gradients and unphysical system behavior. Alternatively the absence of periodic boundary conditions can be compensated by employing a boundary force. This boundary force is required in order to exert the correct mean pressure on the MD system and to minimize the local disturbances in flow quantities such as density and temperature. A number of boundary force models have been employed in hybrid schemes for the simulation of dense fluids [7–10,23,24]. In this work we employ the boundary model that has been proposed by [11] and which was shown to outperform all related works in maintaining a constant density in the atomistic part of the domain. The present boundary force accounts for the local structure of the fluid, which for a monatomic fluid is described by the radial distribution function $g(r)$. In this model we integrate the force components normal to the wall and the potential energy contributions weighted by $g(r)$ over the part of the cutoff sphere that lies outside of the atomistic domain (see Fig. 2). We obtain

$$F_b(r_w) = -2\pi\rho_n \int_{z=r_w}^{r_c} \int_{x=0}^{\sqrt{r_c^2-z^2}} g(r)\frac{\partial U_{12-6}(r)}{\partial r}\frac{z}{r}xdxdz, \tag{14}$$

$$U_b(r_w) = 2\pi\rho_n \int_{z=r_w}^{r_c} \int_{x=0}^{\sqrt{r_c^2-z^2}} g(r)U_{12-6}(r)xdxdz, \tag{15}$$

where r_c is the cutoff radius, ρ_n is the average number density, $r=\sqrt{x^2+z^2}$, and r_w is the distance to the wall.

The $F_b(r)$ and $U_b(r)$ for a Lennard-Jones fluid can be obtained by either using an available parametrization of $g(r)$ as proposed in [25] and performing the integration in (14) and (15) or by evaluating the integrals (14) and (15) explicitly in a separate simulation. We note that the proposed boundary force does not guarantee that particles would not exit the boundary of the atomistic domain. Hence in addition to the boundary force, we employ a hard specular wall that moves with the local fluid velocity. At the end of each time step these walls are reset to their initial positions to maintain a fixed frame of reference. As a consequence some particles

may remain outside the computational domain and are reinserted in regions of inflow. Their final position after reinsertion is determined using the Usher algorithm [26]. In this way we maintain a constant number of particles and minimize the disturbances in the potential energy of the system [11].

MD velocities are sampled in cells of the same size as the cells in the LB domain and they are imposed as boundary conditions on the continuum using two coupling methods for Eq. (13). The first method follows Werder *et al.* and amounts to imposing MD velocities within the one cell wide strip located at a distance δ_s of the MD subdomain, see Fig. 1. This velocity-coupling (VC) approach is enhanced by a coupling method which imposes MD velocities on every common cell except within a strip of width δ_s close to the boundary (see Fig. 1). The multiple velocity couplings amount to approximate coupling of velocity gradients coupling (VGC). We shall observe below that using the VGC approach leads to a closer match with MD reference solutions than when using the VC method. We note here that the width δ_s controls the rate of convergence of the hybrid system and determines its efficiency.

A summary of a Schwarz iteration procedure is the following:

(1) *Continuum simulation*. Solution of the continuum velocity field subject to external (outer boundary) and internal (from the MD) boundary conditions. The internal boundary conditions are imposed either through the VGC or the VC.

(2) *MD simulation*.

(a) Compute the interactions between the atoms including the wall boundary force.

(b) Impose on the MD system the velocity boundary condition obtained from the continuum simulation. Move the atoms.

(c) Move the walls, bounce the atoms that have hit them and reset them to their initial position to keep a constant frame of reference.

(d) Reinsert the particles that have left the domain.

(e) Measure the velocities inside the whole MD subdomain and provide them to the continuum solver (VGC) or measure the velocities only within a one cell wide strip located at a distance δ_s from the wall (VC).

III. RESULTS

We first consider the flow past a CNT embedded normal to the flow direction in order to compare our results with [11]. We note that this flow is nominally two dimensional. In order to test the algorithm in a three-dimensional flow we simulate the flow of liquid argon through a short CNT embedded parallel to the flow direction.

A. Flow past a nanotube

We apply the hybrid LB-MD algorithm to the case of the flow of argon around a CNT centered along the z axis within a $30\times30\times4.254$ nm^3 domain Ω. The CNT is of chirality (16,0) with a radius of $r=0.625$ nm. We choose the density of argon $\rho_{\mathrm{Ar}}=1008$ kg m^{-3} and the temperature $T=215$ K. This corresponds to the dimensionless state point $(T^*,\rho^*)=(1.8,0.6)$ where $T^*=k_BT\epsilon_{\mathrm{ArAr}}^{-1}\mathcal{A}$ and $\rho^*=\rho\sigma_{\mathrm{ArAr}}^3 m_{\mathrm{Ar}}^{-1}\mathcal{A}$. We let k_B be the Boltzmann constant, $m_{\mathrm{Ar}}=0.039\,94$ kg mol^{-1} the atomic mass of argon, and $\mathcal{A}$ Avogadro's number.

The MD domain size is $10\times10\times4.254$ nm^3 centered around the CNT which is subdivided into $20\times20\times1$ sampling cells where 6465 argon atoms are initially equilibrated for 0.2 ns. The width of the strip around the boundary on which both MD and LB are simulated is $\delta_s=2.5$ nm.

We consider an LB domain of size $60\times60\times1$ covering the entire domain where lattice nodes are centered on the corresponding MD sampling cells. The viscosity of the LJ fluid is a parameter of the LB model and set to $\nu=0.745\times10^{-7}$ m^2 s^{-1} [18]. We have performed a sensitivity analysis by increasing and decreasing the viscosity by 5% and found it to be a robust parameter with respect to accuracy. Dirichlet boundary conditions $u_\infty=u_x=100$ ms^{-1} are imposed at the inlet $x=0$ nm and outlet $x=30$ nm. This high velocity is chosen to reduce the number of sampling iterations. The temperature is controlled by using a Berendsen thermostat [19] with a time constant $\tau_T=0.1$ ps. We apply it cellwise in all directions in the boundary cells where the velocity is prescribed and only in the z direction in other cells. The hybrid model is run for 100 cycles which consists of running the LB simulation for 7 ns (15 000 iterations) followed by an MD step equilibrating for 0.2 ns (20 000 iterations) and sampling for $t_s=0.4$ ns. We discuss below how t_s affects the convergence of the results.

Figure 3 shows a comparison between hybrid converged solutions and an MD reference solution over the entire domain. The latter involves 58 198 argon atoms and the temperature is controlled as in the MD subdomain. The reference MD velocity field is sampled over 20 ns. A qualitative match with the reference MD solution is obtained when using the VC approach. The match between the hybrid solution and the reference MD solution becomes quantitative when using the VGC method. This is due to the fact that velocity gradients are not let free but implicitly imposed. A consequence of this is that discrepancies in the wake and on the sides of the CNT that appear when using the VC approach, and also reported in [11], are not observed when using the VGC method.

Figure 4 shows the evolution of the norm of the velocity along the $y=15$ nm and $x=15$ nm plane. The system starts from a constant initial condition $u_x=u_\infty=100$ ms^{-1}. This unphysical state leads to the formation of high velocity regions around the CNT. They then slowly spread out on the sides of the tube and increase the side velocity. Considering the VGC approach, we observe that the velocity upstream and downstream adjusts smoothly to the reference solution. The situation is different when employing the VG method. Indeed the hybrid velocity profiles show deviations from the MD reference solution especially downstream from the CNT. It is worth noting that we get identical results when initializing the system with initial conditions closer to the steady solution.

In agreement with [20], we observe that argon flow past a CNT normal to the flow results in a vanishing velocity at the surface of the CNT. In this particular configuration, the velocity boundary condition around the tube can therefore be approximated by a no-slip condition allowing us to solve the

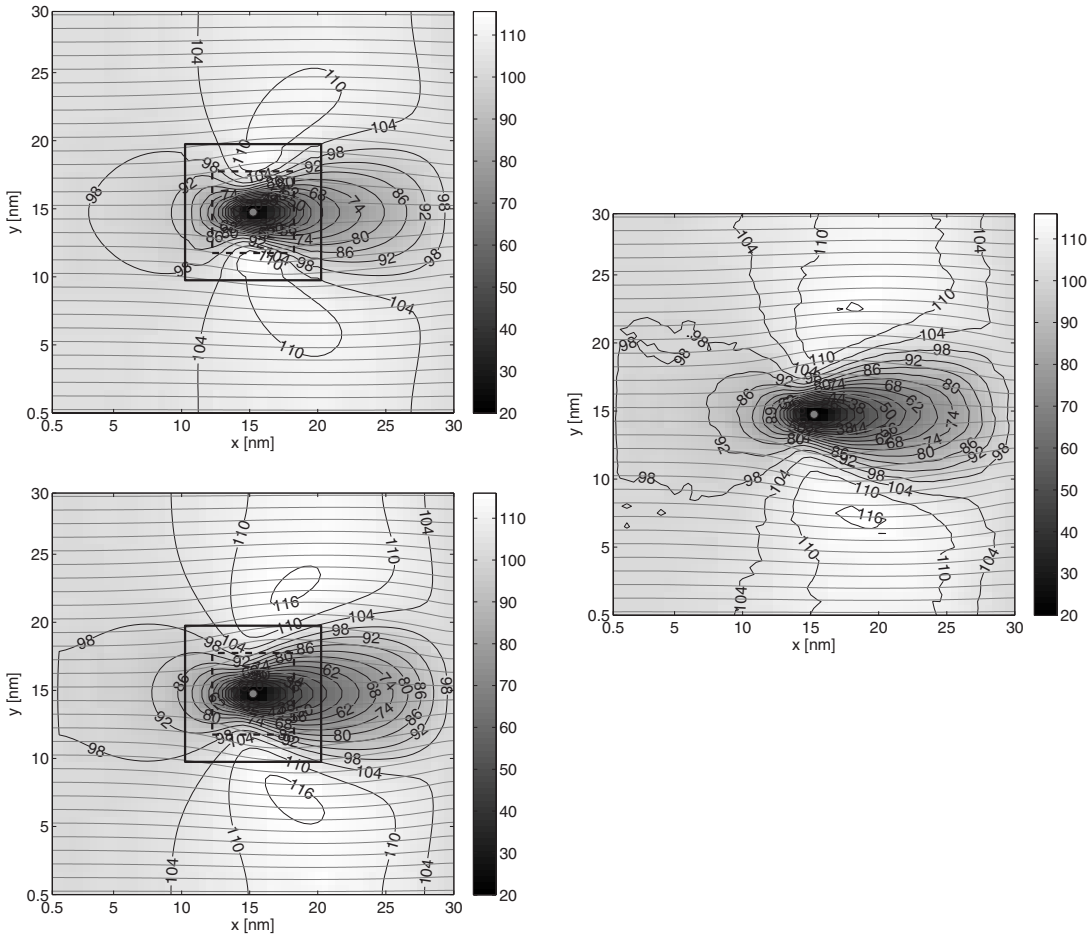

FIG. 3. (Left-hand side) Converged hybrid and (right-hand side) reference MD solutions of a flow past a CNT. (Top left-hand side) Velocities and (bottom left-hand side) velocities and velocity gradients are imposed from the MD to the continuum. The scale and contour lines depict the norm of the velocity expressed in ms^{-1}. Gray lines are streamlines. The thick squares represent (solid lines) the boundary of the MD domain and (dashed lines) the boundary of the overlapping region.

NS equations. Figure 4 shows LB velocity profiles where the CNT is modeled off-lattice using an immersed boundary technique [21]. We will see however that this approximation is not applicable when we consider a CNT with a different orientation.

We quantify the convergence towards the reference MD solution by defining an error e^j between the hybrid solution at cycle j and the reference MD solution as

$$e^j = \frac{1}{N} \sum_{k \in \Omega} \frac{|\mathbf{u}_k^j - \mathbf{u}_{k,\mathrm{MD}}|}{u_\infty}, \tag{16}$$

where N is the number of cells in Ω, $\mathbf{u}_k^j$ and $\mathbf{u}_{k,\mathrm{MD}}$ are, respectively, the hybrid and reference MD velocities at cycle j in the cell k.

Figure 5 shows the time evolution of the error which rapidly decays during the first 10 cycles. The error then fluctuates around an average value which is a function of the sampling time t_s. Considering the VGC approach, we measure an average error between cycle 50 and 100 of 1.3% for $t_s = 0.4$ ns and $t_s = 0.8$ ns and an average error of 1.9% for $t_s = 0.2$ ns. We observe in Fig. 5 that considering short t_s leads to undesirable fluctuations whereas long t_s decreases the computational efficiency of the model. An optimum is found to be $t_s = 0.4$ ns assumed hereafter if not otherwise specified. Figure 5 also shows the time evolution error when using the VC method. The average error over the last 50 cycles is 3.8% and is comparable to the error evolution reported in [11].

The pointwise error between the hybrid and the reference MD solutions is depicted in Fig. 5. Using the VGC technique leads to a localized and maximum 3.9% error region showing only on one side of the CNT. Everywhere else the error is up to 2.5%. The error is higher when using the VC approach where we observe a large error of up to 15% in the wake.

The supercritical state point $(T^*, \rho^*) = (1.8, 0.6)$ is associated with less structural correlations than in a liquid state. In order to assess their effect on the convergence we have considered the liquid state point $(131\ \mathrm{K}, 1361\ \mathrm{kg\ m^{-3}}) = (1.09, 0.81)$ related to the kinematic viscosity $\nu = 1.42 \times 10^{-7}\ \mathrm{m^2\ s^{-1}}$ [18]. For similar parameters as for the state points (1.8,0.6), we measure an error of 2.0% between the hybrid solution and the associated reference MD solution. The error is slightly higher than the one obtained in the supercritical state and indicates that the LB-MD model can also be applied when considering liquid states.

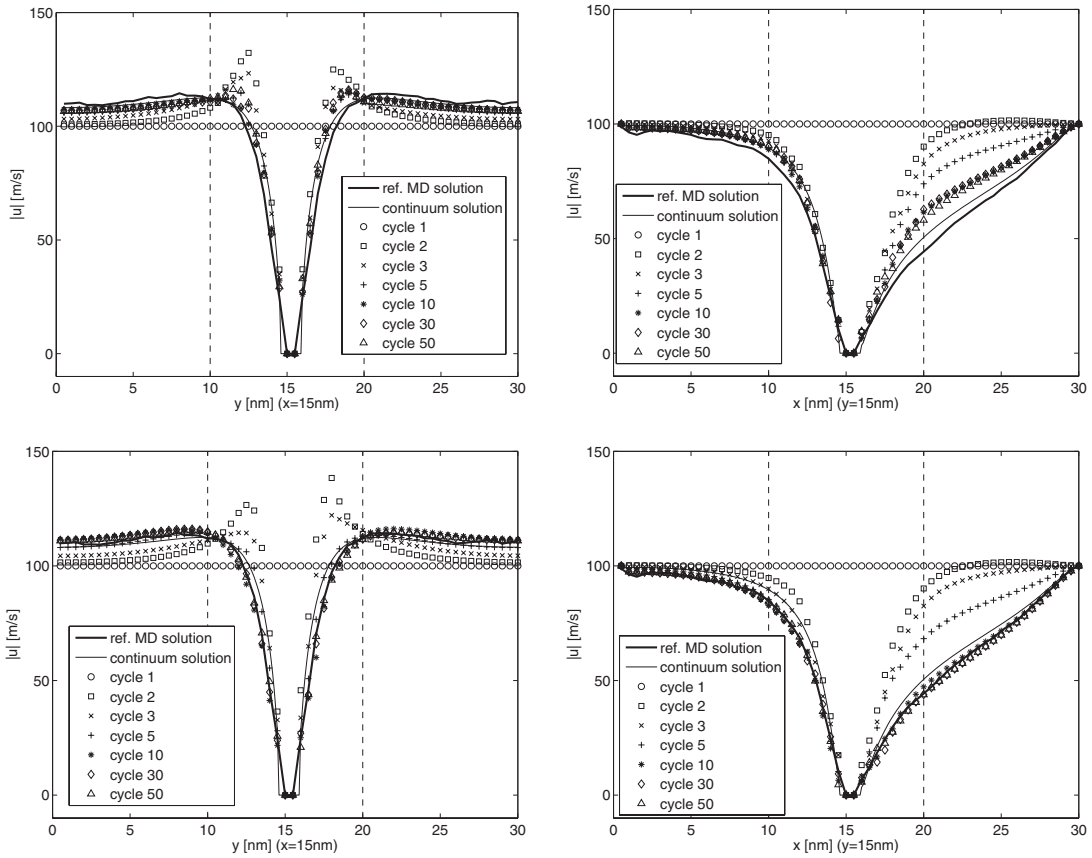

FIG. 4. Evolution of the hybrid profiles of the norm of the velocity in the planes located (left-hand side) at $x=15$ nm and (right-hand side) at $y=15$ nm. (Top) Velocities (bottom) and velocity gradients are imposed. The solid thick line is the reference MD solution whereas the solid line is the continum solution where no-slip boundary condition is considered around the CNT. Hybrid solutions are plotted after a various number of cycles. Dashed lines represent the boundaries of the MD domain. The additional exchange of velocity gradient information improves the results.

B. Flow through a nanotube

We now consider the three-dimensional flow through a CNT driven by a constant velocity $u_x=100$ ms^{-1} applied at $x=0$ and $x=28$ nm. The CNT is centered along the x axis in a domain of size $28\times16\times16$ mm^3 and it is of chirality $(16,0)$ with a length $l=2.34$ nm. We choose the dimensionless state point $(T^*,\rho^*)=(1.8,0.6)$.

The MD subdomain size is $14\times10\times10$ nm^3 centered around the CNT and is subdivided into $14\times10\times10$ sampling cells. 21 278 argon atoms are initially equilibrated for 0.2 ns and $\delta_s=3$ nm. The temperature is regulated by applying a Berendsen thermostat cellwise in every direction within the boundary cells. We consider a $28\times16\times16$ LB domain covering the entire domain where lattice nodes are centered in corresponding sampling cells. MD and LB domains are coupled via the VGC approach. The hybrid model ran for 50 cycles consisting of running the LB simulation for 13.4 ns (15 000 iterations) followed by an MD step equilibrated for 0.2 ns and sampled for $t_s=0.4$ ns.

Figure 6 shows a comparison between the hybrid and the reference MD solution. The latter consists of 108 943 argon atoms sampled for 20 ns where thermal boundary conditions are as in the MD subdomain. There is an overall good quantitative agreement between the solutions. We observe regions above and under the CNT where the hybrid velocity is slightly faster than in the reference MD solution. The difference is at most 4%. We quantify the overall agreement by measuring average errors following Eq. (16) over different regions and during the last 30 cycles and obtain a global error $e_g=2.6\%$ over the whole domain and a local error $e_l=2.1\%$ in the tube.

The rather small diameter of the CNT leads to a higher argon density within the tube. We measure a 7% increase that cannot be described by the incompressible NS equations. This issue could however be alleviated by considering a compressible LB model [22].

In this conformation, the velocities around the CNT are nonzero. The corresponding continuum velocity boundary condition is unknown and is a function of the system parameters [20]. A continuum solution approximating the reference solution is therefore unfeasible.

The computational efficiency of the LB-MD model is estimated by comparing the time needed to update the dynamics of the atoms past the nanotube at each MD step of the reference (t_{ref}) and hybrid (t_{hyb}) solution, respectively. We measure $t_{\text{ref}}=0.56$ s and $t_{\text{hyb}}=0.08$ s in the case of the flow past a CNT. The hybrid solution is computed $R=0.56/0.08=7$ times faster than the reference solution. We get a ratio $R=1.04/0.43=2.4$ in the case of a flow through a CNT. Ra-

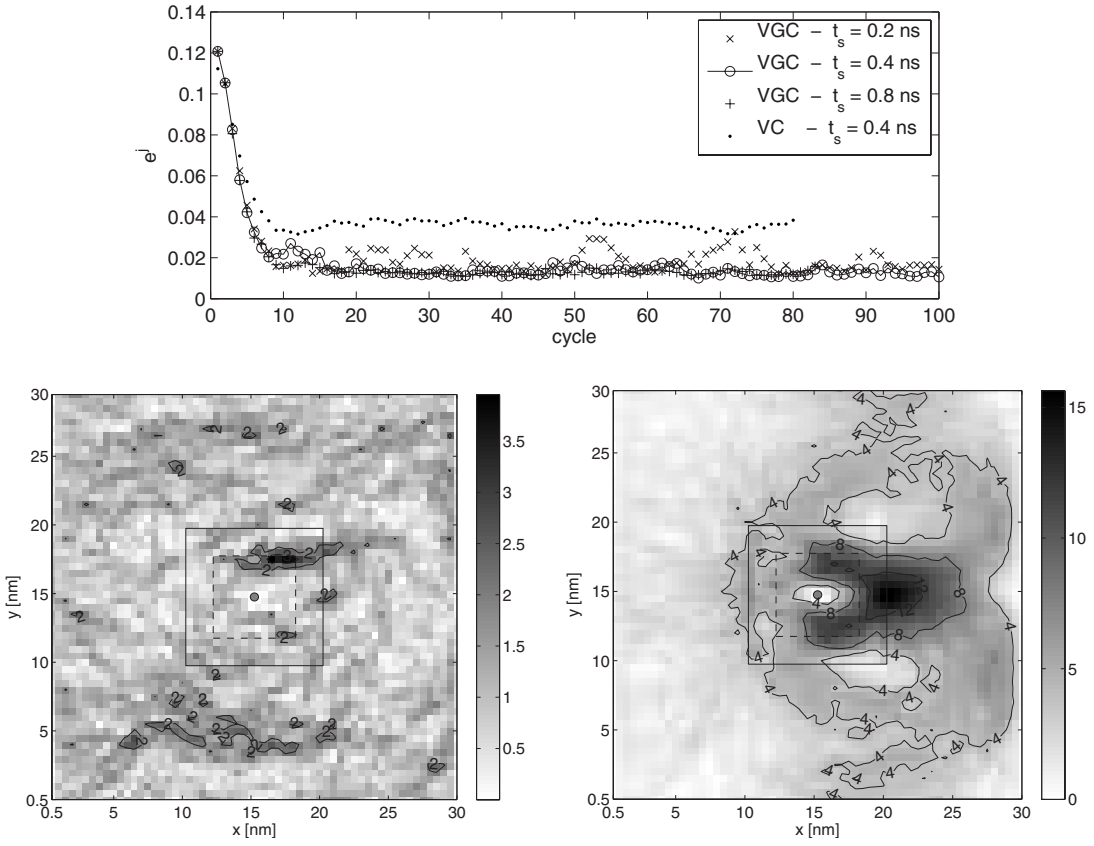

FIG. 5. (Top) Evolution of the error e^j between the hybrid solution and the reference MD solution. Different sampling time t_s and coupling techniques are considered. In the case of VGC the error reaches a plateau (top) 3 times smaller than in the VC approach. (Bottom) Pointwise error according to Eq. (16) shown in percentage and averaged between cycle 50 and 100. The sampling time (t_s) is 0.4 ns. (Left-hand side) The VGC and (right-hand side) the VC techniques are used. We observe the significant improvement through the application of the VGC approach.

tios R are of the same order as the volume ratio between the whole computational domain and MD domain. This is because, as in every hybrid model, MD is typically two orders of magnitude faster than LB and because the MD computation time is linearly proportional to the numbers of atoms, i.e., to the volume of the domain. Small systems have been chosen here in order to compare hybrid to reference solutions. Considering larger systems would exhibit much higher

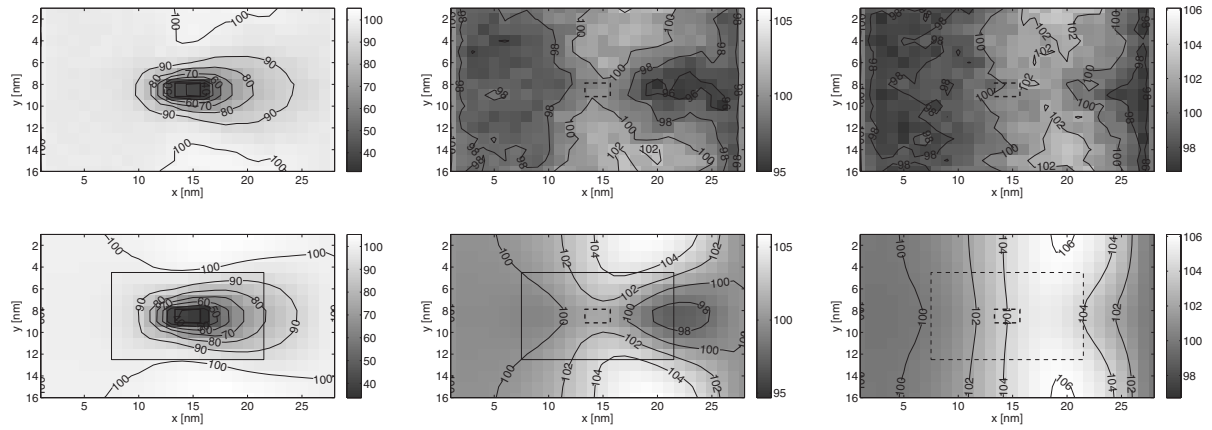

$z = 8$ nm $z = 4$ nm 0 nm

FIG. 6. Reference MD (top) and hybrid (bottom) solutions of the flow through a CNT driven by a constant velocity u_x=100 ms^{-1} applied at x=0 nm and x=28 nm. The norm of the velocity is plotted. Each column corresponds to a different x-y plane at z=8 (left-hand side), 4 (middle), and 0 nm (right-hand side). Contour lines are plotted and expressed in ms^{-1}. Bold and thin rectangles depict the CNT and the MD domain, respectively.

ratios. For example, nanodevices ($\propto 10^3$ nm^3) embedded in microscale systems ($\propto 1$ μm^3) would lead to ratios of the order of 10^6.

IV. CONCLUSION

We have presented a hybrid model coupling a lattice Boltzmann solution of the incompressible Navier-Stokes equations to a molecular dynamics simulation of a dense fluid, using a Schwarz domain decomposition technique. The two descriptions are coupled via an exchange of velocities (VC) or velocity gradients (VGC). The applicability of the method was demonstrated in two- and three-dimensional flows of liquid argon past carbon nanotubes normal and aligned with the flow velocity.

We have first computed the flow past a CNT with an axis normal to the flow velocity. Using the VGC approach we observed quantitative agreement between the hybrid and the reference MD solutions with an average error of 1.3% that provides an improvement over previously reported results [11] for the same configuration. We attribute this improvement to the fact that we match the velocity field within a wider region rather than along a one cell strip implying that velocity gradients and in turn shear forces are implicitly matched in the two descriptions. We also show that the velocity vanishes around the tube in this conformation making a continuum solution a good approximation of the reference solution. This is not the case however when considering the flow through a CNT. The transport of argon in the CNT is captured within 2.1% with the present LB-MD model.

In addition of being a tool to help investigating multiscale physics by considerably reducing an otherwise prohibitive computational time, this approach largely extends the applicability of LB models by providing us with fully microscopic boundary conditions.

ACKNOWLEDGMENT

The authors wish to thank P.G. Gonnet for many helpful technical discussions.

[1] R. J. Chen, S. Bangsaruntip, K. A. Drouvalakis, N. W. S. Kam, M. Shim, Y. M. Li, W. Kim, P. J. Utz, and H. J. Dai, Proc. Natl. Acad. Sci. U.S.A. **100**, 4984 (2003).
[2] J. Li, H. T. Ng, A. Cassell, W. Fan, H. Chen, Q. Ye, J. Koehne, J. Han, and M. Meyyappan, Nano Lett. **3**, 597 (2003).
[3] Y. Lin, S. Taylor, H. Li, K. A. Fernando Shiral, L. Qu, W. Wang, L. Gu, B. Zhou, and Y.-P. Sun, J. Mater. Chem. **14**, 527 (2004).
[4] M. Zheng, A. Jagota, E. D. Semke, B. A. Diner, R. S. McLean, S. R. Lustig, R. E. Richardson, and N. G. Tassi, Nat. Mater. **2**, 338 (2003).
[5] K. Watanabe, T. Takayama, S. Ogata, and S. Isozaki, AIChE J. **49**, 1956 (2003).
[6] J. Koplik and J. R. Banavar, Annu. Rev. Fluid Mech. **27**, 257 (1995).
[7] S. T. O'Connell and P. A. Thompson, Phys. Rev. E **52**, R5792 (1995).
[8] N. G. Hadjiconstantinou and A. T. Patera, Int. J. Mod. Phys. C **8**, 967 (1997).
[9] E. G. Flekkøy, G. Wagner, and J. Feder, Europhys. Lett. **52**, 271 (2000).
[10] X. B. Nie, S. Y. Chen, W. N. E, and M. O. Robbins, J. Fluid Mech. **500**, 55 (2004).
[11] T. Werder, J. H. Walther, and P. Koumoutsakos, J. Comput. Phys. **205**, 373 (2005).
[12] P. Koumoutsakos, Annu. Rev. Fluid Mech. **37**, 457 (2005).
[13] X. B. Nie, S. Y. Chen, and M. O. Robbins, Phys. Fluids **16**, 3579 (2004).
[14] S. Succi, *The Lattice Boltzmann Equation, For Fluid Dynamics and Beyond* (Oxford University Press, Oxford, 2001).
[15] Z. Guo, C. Zheng, and B. Shi, Phys. Rev. E **65**, 046308 (2002).
[16] B. Chopard and M. Droz, *Cellular Automata Modeling of Physical Systems* (Cambridge University Press, Cambridge, 1998).
[17] B. F. Smith, P. E. Bjorstad, and W. D. Gropp, *Domain Decomposition. Parallel Multilevel Methods for Elliptic Partial Differential Equations* (Cambridge University Press, Cambridge, 1996).
[18] K. Meier, A. Laesecke, and S. Kabelac, J. Chem. Phys. **121**, 3671 (2004).
[19] H. J. C. Berendsen, J. P. M. Postma, W. F. van Gunsteren, A. DiNola, and J. R. Haak, J. Chem. Phys. **81**, 3684 (1984).
[20] J. H. Walther, T. Werder, R. L. Jaffe, and P. Koumoutsakos, Phys. Rev. E **69**, 062201 (2004).
[21] A. Dupuis and P. Koumoutsakos, J. Comput. Phys. (unpublished).
[22] A. J. Briant, A. J. Wagner, and J. M. Yeomans, Phys. Rev. E **69**, 031602 (2004).
[23] R. Delgado-Buscalioni and P. V. Coveney, Phys. Rev. E **67**, 046704 (2003).
[24] N. G. Hadjiconstantinou, J. Comput. Phys. **154**, 245 (1999).
[25] E. Matteoli and G. Ali Mansoori, J. Chem. Phys. **103**, 4672 (1995).
[26] R. Delgado-Buscalioni and P. V. Coveney, J. Chem. Phys. **119**, 978 (2003).